J|A|C|S
ARTICLES

Published on Web 07/10/2008

Mechanistic Consequences of Composition in Acid Catalysis by Polyoxometalate Keggin Clusters

Josef Macht,[†] Michael J. Janik,[‡] Matthew Neurock,[§] and Enrique Iglesia*,[†]

Department of Chemical Engineering, University of California at Berkeley, Berkeley, California 94720, Department of Chemical Engineering, Pennsylvania State University, University Park, Pennsylvania 16802, and Departments of Chemical Engineering and Chemistry, University of Virginia, Charlottesville, Virginia 22904

Received April 27, 2008; E-mail: iglesia@berkeley.edu

Abstract: The kinetics and mechanism of ether and alkanol cleavage reactions on Brønsted acid catalysts based on polyoxometalate (POM) clusters are described in terms of the identity and dynamics of elementary steps and the stability of the transition states involved. Measured rates and theoretical calculations show that the energies of cationic transition states and intermediates depend on the properties of reactants (proton affinity), POM clusters (deprotonation enthalpy), and ion-pairs in transition states or intermediates (stabilization energy). Rate equations and elementary steps were similar for dehydration of alkanols (2-propanol, 1- and 2-butanol, *tert*-butanol) and cleavage of *sec*-butyl-methyl ether on POM clusters with different central atoms (P, Si, Co, Al). Dehydration rates depend on the rate constant for elimination from adsorbed alkanols or ethers and on the equilibrium constant for the formation of unreactive reactant dimers. Elimination involves E1 pathways and late carbenium-ion transition states. This is consistent with small kinetic isotope effects for all deuterated alkanols, with strong effects of substituents on elimination rates, and with the similar alkene stereoselectivities measured for alkanol dehydration, ether cleavage, and alkene double-bond isomerization. *n*-Donor reactants (alkanols, ethers) and products (water) inhibit dehydration rates by forming stable dimers that do not undergo elimination; their stability is consistent with theoretical estimates, with the dynamics of homogeneous analogues, and with the structure and proton affinity of the *n*-donors. Elimination rate constants increased with increasing valence of the central POM atom, because of a concurrent decrease in deprotonation enthalpies (DPE), which leads to more stable anionic clusters and ion-pairs at transition states. The DPE of POM clusters influences catalytic rates less than the proton affinity of the alkene-like organic moiety at the late carbenium-ion-type transition states involved. These different sensitivities reflect the fact that weaker acids typically form anionic clusters with a higher charge density at the transition state; these clusters stabilize cationic fragments more effectively than those of stronger acids, which form more stable conjugate bases with lower charge densities. These compensation effects are ubiquitous in acid chemistry and also evident for mineral acids. The stabilization energy and the concomitant charge density and distribution in the anion, but not the acid strength (DPE), determine the kinetic tolerance of *n*-donors and the selectivity of reactions catalyzed by Brønsted acids.

1. Introduction

Polyoxometalate (POM) clusters with stable Keggin structure exhibit well-defined size, atomic connectivity, and structures, which allow changes in their composition without concomitant structural consequences, reliable quantum chemical treatments, and the analysis of composition−function relations using experiments and theory without distractions from concurrent changes in structural motifs. Their specific functions as acid and oxidation catalysts are well-known,[1–3] rendering these reactions well-suited to address the effects of composition on electronic structure and catalytic function.

In a previous communication,[4] we reported preliminary data on the effects of the identity of the central atom X (P, Si, Al, and Co) in SiO_2-supported Keggin-type POM clusters ($H_{8-n}X^{n+}W_{12}O_{40}\equiv H_{8-n}XW$) for the catalytic dehydration of 2-butanol. These data showed that turnover rates reflect the rate constant for C−O cleavage via carbenium-type transition states and the equilibrium constant for formation of unreactive 2-butanol dimers (Scheme 1). These conclusions are consistent with experimental evidence and with density functional theory (DFT) descriptions of the energetics of proposed elementary steps.

Rate and equilibrium constants increased in parallel with increasing valence of the central atom X, as the deprotonation enthalpy (DPE)—a rigorous descriptor of acid strength available

[†] University of California.
[‡] Pennsylvania State University.
[§] University of Virginia.

(1) Okuhara, T.; Mizuno, N.; Misono, M. *Adv. Catal.* **1996**, *41*, 133.
(2) Mizuno, N.; Misono, M. *Chem. Rev.* **1998**, *98*, 199.
(3) Hill, C. L.; Prosser, C. M. *Coord. Chem. Rev.* **1995**, *143*, 407.
(4) Macht, J.; Janik, M. J.; Neurock, M.; Iglesia, E. *Angew. Chem., Int. Ed.* **2007**, *46*, 7864.
(5) Cowan, J. J.; Hill, C. L.; Reiner, R. S.; Weinstock, I. A. *Inorg. Synth.* **2002**, *33*, 18.

Scheme 1. Proposed Sequence of Elementary Steps for 2-Butanol Dehydration on POM Clusters with Keggin Structure

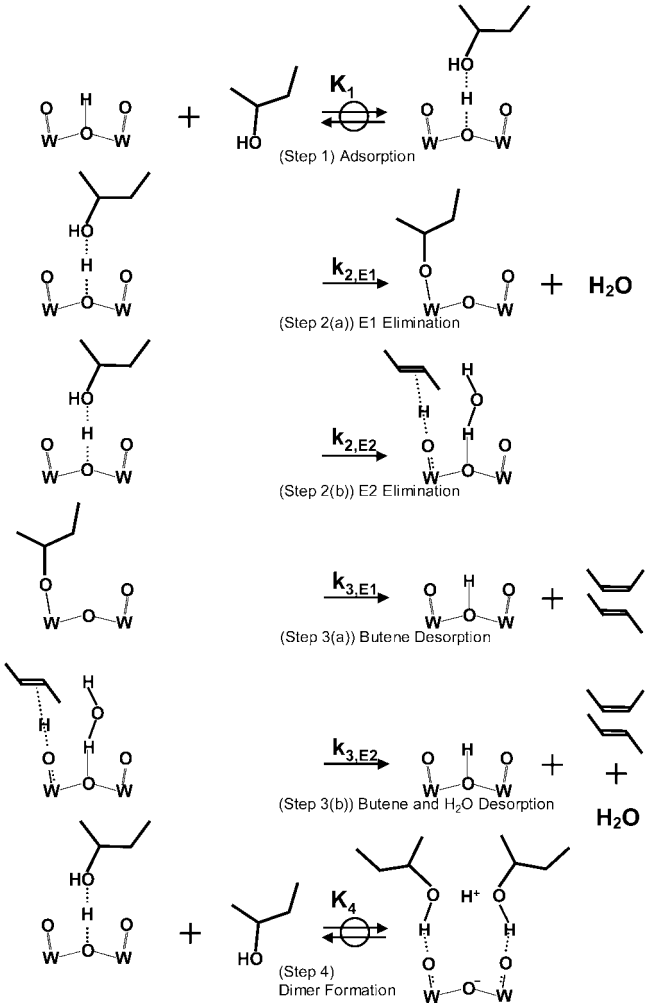

from DFT calculations—concurrently decreased. These trends reflect the cationic nature of activated complexes and unreactive butanol dimers, species that require effective charge stabilization by anionic Keggin clusters. Here, we discuss the detailed mechanism of R_1-OR_2 cleavage reactions and show that carbenium-ion-type transition states in the kinetically relevant elimination step and the kinetic inhibition by *n*-donors, such as alkanol or ether reactants and H_2O products—the solvation of intermediates in acid catalysis, apply generally to R_1-OR_2 cleavage reactions catalyzed by strong Brønsted acids.

Our previous communication reported the relation between DPE and rate constants. Herein, we quantitatively account for the stability of activated complexes in terms of the deprotonation enthalpy (DPE) of acid POM clusters, the dehydration enthalpy of protonated alkanol reactants, and the ion-pair stabilization energy, consistent with Born−Haber thermochemical cycles. Elimination rate constants and barriers, however, are more sensitive to the properties of the reactants than to those of the clusters, because the stabilization of the ion-pair at the transition state becomes more favorable with increasing POM deprotonation enthalpy as a consequence of the concurrent increase in the charge density on the anionic fragment. The identity of the acid leads not only to differences in acid strength but also to differences in ion-pair stabilization, caused by, for example, the charge densities and distributions of the anionic conjugate base. We show that differences in ion-pair stabilization and not acid strength (DPE) itself determine the kinetic tolerance of a given acid to the presence of water and other *n*-donors, and the selectivity in reaction networks catalyzed by Brønsted acids.

We provide evidence for concepts essential to guide the design of materials for acid-catalyzed rearrangements of oxygenates and hydrocarbons ubiquitous in the conversion of fossil and biomass resources to chemicals and fuels. These conclusions are valid in general for reactions involving cationic intermediates and transition states and are not restricted to alkanol and ether cleavage reactions and to polyoxometalate clusters, which are chosen here merely because their structural fidelity and diverse compositions allow the experimental and theoretical clarification of these concepts.

Table 1. Elemental Composition, POM Content, POM Surface Density and Notation Used for All Samples

composition	POM content (% wt)	surface density (POM nm^{-2})[a]	notation
$H_3PW_{12}O_{40}/SiO_2$	40	0.5	$0.5H_3PW/SiO_2$
	20	0.19	$0.19H_3PW/SiO_2$
	10	0.08	$0.08H_3PW/SiO_2$
	5	0.04	$0.04H_3PW/SiO_2$
$H_4SiW_{12}O_{40}/SiO_2$	40	0.5	$0.5H_4SiW/SiO_2$
	20	0.19	$0.19H_4SiW/SiO_2$
	10	0.08	$0.08H_4SiW/SiO_2$
	5	0.04	$0.04H_4SiW/SiO_2$
$H_5AlW_{12}O_{40}/SiO_2$	5	0.04	$0.04H_5AlW/SiO_2$
$H_6CoW_{12}O_{40}/SiO_2$	5	0.04	$0.04H_6CoW/SiO_2$

[a] Estimated from the POM content and the BET surface area of the samples.

2. Experimental Methods

2.1. Catalyst Synthesis. $H_3PW_{12}O_{40}$ (Aldrich), $H_4SiW_{12}O_{40}$ (Aldrich, 99.9%), $H_5AlW_{12}O_{40}$ (prepared as in ref 5) and $H_6CoW_{12}O_{40}$ (prepared as in refs 6, 7) clusters were deposited onto SiO_2 (Cab-O-Sil, 304 $m^2\ g^{-1}$, 1.5 $cm^{-3}\ g^{-1}$ pore volume; washed three times in 1 M HNO_3 and treated in dry air (Praxair, UHP, 573 K, 5 h, 20 $cm^3\ g^{-1}$)) by incipient wetness impregnation of their respective solutions (1.5 $cm^3\ g^{-1}$ dry SiO_2) in ethanol (Aldrich, anhydrous 99.5%)). The impregnated samples were treated in flowing dry air (Praxair, UHP, 20 $cm^3\ g^{-1}$) at 323 K for 24 h; holding these samples in a closed vial for two days afterward enabled the redistribution of the POM clusters to obtain a uniform concentration profile.[8] The structural integrity of the supported POM clusters has been established by NMR (see Supporting Information for details). The composition, POM content (% wt), and POM surface densities (POM nm^{-2}) are shown in Table 1. The nomenclature used lists the surface density (as POM nm^{-2}) and the respective compositions in abbreviated form ($H_3PW_{12}O_{40} \rightarrow H_3PW$) with the support material noted immediately thereafter (e.g., $0.19H_3PW/SiO_2$).

2.2. Alkanol and Ether Elimination Rates and Selectivities. Catalytic rates and selectivities were measured at 333−373 K in a quartz flow cell (1.0 cm inner diameter) containing 1−200 mg of catalysts (125−180 μm); samples smaller than 20 mg were diluted with acid-washed quartz (125−180 μm) to give 50 mg of the mixture. Samples were held onto a porous quartz disk and temperatures were measured using K-type thermocouples placed in a well on the outside of the quartz reactor immediately above the catalyst bed. Temperatures were kept constant (±0.2 K) using a Watlow controller (Series 982) and a resistively heated furnace.

(6) Baker, L. C. W.; McCutcheon, T. P. *J. Am. Chem. Soc.* **1956**, *7878*, 4503.
(7) Baker, L. C. W.; Love, B.; McCutcheon, T. P. *J. Am. Chem. Soc.* **1950**, *72*, 2374.
(8) Lee, S. Y.; Aris, R. *Catal. Rev., Sci. Eng.* **1985**, *27*, 207.

Thermal treatments in He (Praxair, UHP) or air (Praxair, extra-dry) (80 cm^3 min^{-1}) up to 573 K before reaction did not influence measured rates. Transfer lines were held at 393 K to prevent adsorption or condensation of reactants, products, or titrants before their chromatographic analysis. Alkanol and ether reactants (Sigma-Aldrich, 99.5% (2-butanol), 99.8% (1-butanol), 99% (1-butanol-d_{10}), 99.5% (*tert*-butanol, anhydrous), 99.5% (2-propanol), 99.5% (2-propanol-d_8), 99% (2-propanol-d_6), 99% (*sec*-butyl methyl ether)) and H_2O (18 MΩ cm^{-1}, deionization) were used without additional purification and introduced as a liquid using a syringe pump (Cole Parmer, 74900 series) by vaporization into flowing He (Praxair, UHP) at 393 K. Molar rates of 1-butene (Scott Specialty Gases, 99%), He, and all gaseous species were adjusted to give the desired reactant pressures and to maintain low and relatively constant reactant conversions (<10%). Reactant and product concentrations were measured by gas chromatography using flame ionization detection (Agilent 6890N GC, 50 m HP-1 column). Only alkene products of dehydration reactions were detected (1-butene, *cis*-2-butene, *trans*-2-butene, 2-methlypropene, propene) during 1-butanol, 2-butanol, *tert*-butanol, and 2-propanol dehydration. Deactivation by oligomerization reactions was avoided by the low alkanol conversion and the concomitantly low alkene pressures and low alkoxide surface concentrations. 1-Butene, *cis*-2-butene, *trans*-2-butene, methanol and dimethyl ether were detected during *sec*-butyl-methyl ether cleavage reactions. Double-bond isomerization reactions of 1-butene led to *cis*-2-butene and *trans*-2-butene products. Brønsted acid sites were titrated by introducing pyridine (Aldrich, 99.9%) dissolved in 2-butanol reactants (Sigma-Aldrich, 99.5%, anhydrous) into flowing He and vaporized at 373 K to give a stream containing 0.5 kPa 2-butanol and 0.9 Pa pyridine. The amount of titrant adsorbed on the catalyst was measured from its residual concentration in the effluent stream using the same chromatographic protocols as for catalytic reactions.

2.3. Theoretical Calculations and Methods. Density functional calculations were performed using the Gaussian 03 program.[9] Geometries were optimized and energies calculated at the B3LYP/6-31+G(d,p) level of theory.

3. Results and Discussion

3.1. Kinetics and Mechanism of R_1-OR_2 Cleavage Reactions. Figure 1 shows rates for 2-butanol dehydration on H_3PW/Si and H_4SiW/Si and for *sec*-butyl-methyl ether cleavage on H_3PW/Si as a function of reactant pressure. Reaction rates decreased with increasing reactant pressure for both reactants on all POM catalysts (Figure 1). Following, we propose and confirm elementary steps for 2-butanol dehydration consistent with these data; we also conclude from the ubiquitous prevalence of such rate dependences that such steps remain valid for general R_1-OR_2 (where R_i is an alkyl group or H atom) cleavage reactions on POM clusters.

2-Butanol dehydration proceeds via elementary steps consisting of quasi-equilibrated 2-butanol adsorption on Brønsted acid sites via hydrogen bonding (Step 1, Scheme 1) to form 2-butanol "monomers".[4,10] These monomers decompose irreversibly via E1-type or E2-type mechanisms.[11] E2 routes involve concerted cleavage of C−O and C−H bonds in butanol monomers (step 2b, Scheme 1) via H-abstraction from $C_\beta-H$ bonds by basic oxygens and cleavage of protonated $C_\alpha-OH_2^+$ bonds to form adsorbed butene and H_2O molecules. In E1 pathways, the $C_\alpha-OH_2^+$ bond is cleaved to form water molecules and adsorbed butoxides (step 2a, Scheme 1). E1 sequences are completed by deprotonation of adsorbed butoxides (step 3a, Scheme 1) and E2 sequences by desorption of H_2O and butenes (step 3b, Scheme 1).

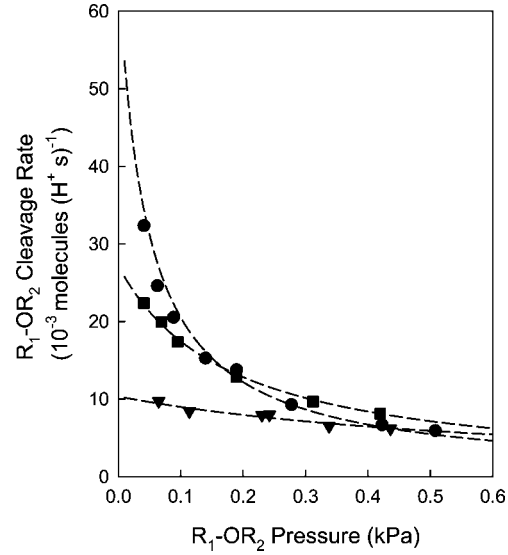

Figure 1. R_1-OR_2 cleavage rates (per H^+) as a function of R_1-OR_2 pressure for $0.04H_3PW/Si$ (●), $0.04H_4SiW/Si$ (■) for 2-butanol dehydration and $0.04H_3PW/Si$ (▼) for *sec*-butyl-methyl ether cleavage reaction (343 K, conversion <10%). Dashed lines represent the prediction from eq 2.

While elimination pathways that led to the cleavage of the C−O and C−H bond in a single step (without alkoxide formation) could be established by DFT for 2-butanol and 1-propanol dehydration, no true E2-type elimination transition state involving concerted C−O bond and C−H bond breaking could be identified, and the elimination transition states resembled a secondary or primary carbenium ion, respectively.[10] The calculated elimination barriers suggest a slight preference for two sequential steps passing through the alkoxide intermediate (barrier 132/138 kJ mol^{-1} (2-butanol/1-propanol)) versus bypassing alkoxide formation (barrier 139/150 kJ mol^{-1} (2-butanol/1-propanol)).[10] The carbenium-ion nature of the transition state in kinetically relevant elimination steps is consistent with the strong effects of substitution at the carbon bearing the OH group, as discussed in section 3.2, the preference of the pathways involving alkoxide intermediates is consistent with elimination stereoselectivities discussed later in this section. Butanol monomers can also interact with another 2-butanol to form protonated dimers, which are stabilized by strong hydrogen bonds $[-O-H\cdots O-]^+$ and rendered unreactive at conditions that cause elimination from unsolvated monomers (step 4, Scheme 1, see also section 3.3).

These elementary steps lead to a rate equation consistent with the measured effects of 2-butanol pressure on dehydration turnover rates (Figure 1), (rate equations derived in Supporting Information):

$$r = \frac{k_2[H^+]}{1 + K_4[C_4H_9OH]} \qquad (2)$$

where k_2 is the elimination rate constant (step 2, Scheme 1, $k_2 = k_{2,E1} + k_{2,E2}$) and K_4 is the equilibrium constant for dimer formation:

$$[C_4H_9OH]H^+_{cat} + [C_4H_9OH]_{gas} \leftrightarrow [C_4H_9OH]_2H^+_{cat} \qquad (3)$$

(9) Frisch, M. J.; et al. *Gaussian 03*, revision C.02; Gaussian Inc.: Wallingford, CT, 2004.
(10) Janik, M. J.; Neurock, M. , in preparation.
(11) Noller, H.; Andreau, P.; Hunger, M. *Angew. Chem., Int. Ed.* **1971**, *10*, 172.

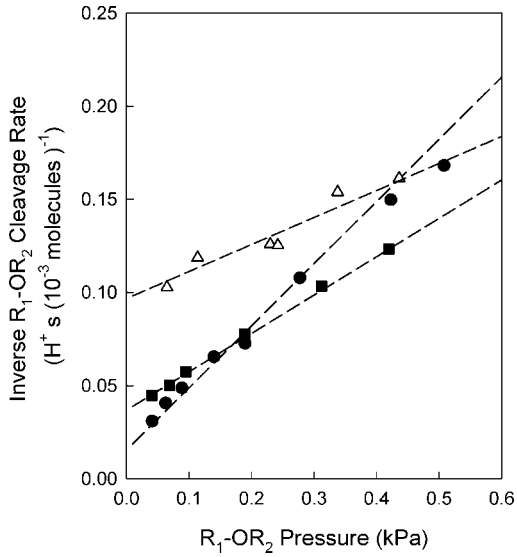

Figure 2. Inverse R_1-OR_2 cleavage rates as a function of R_1-OR_2 pressure for $0.04H_3PW/Si$ (●), $0.04H_4SiW/Si$ (■) for 2-butanol dehydration and $0.04H_3PW/Si$ (Δ) for *sec*-butyl-methyl ether cleavage reaction (343 K, conversion <10%).

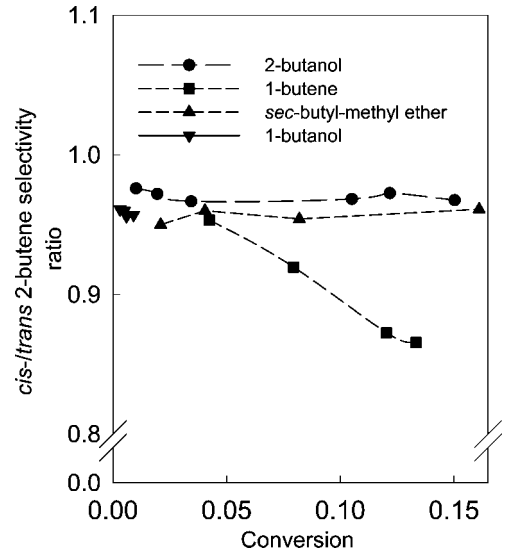

Figure 3. *cis-/trans*-2-Butene selectivity ratios as a function of conversion for 2-butanol dehydration (●), 1-butene double bond isomerization (■), *sec*-butyl-methyl ether decomposition (▲), and 1-butanol dehydration (▼) on $0.04H_3PW/Si$ (343 K).

(also step 4, Scheme 1), while $[H^+]$ is the concentration of accessible protons. Inverse rates are proportional to 2-butanol pressure, as suggested by eq 2, for POM clusters with P, Si, Al, and Co central atoms, as well as for all alkanols and ethers used in this study (Figure 2). In all cases, R_1-OR_2 cleavage rates decreased with increasing R_1-OR_2 pressure. These rates reflect contributions from rate constants for the cleavage step and from equilibrium dimer formation constants, leading to effects of POM composition that depend on reaction conditions when measured rates are simply compared among these catalysts without proper mechanistic interpretation.

The form of eq 2 indicates that R_1-OR_2 monomers and dimers are the most abundant surface species during steady-state catalysis. On $0.04H_3PW/Si$, 1-butene isomerization rate constants were much larger (1.2 (POM s)$^{-1}$) than 2-butanol decomposition rate constants of elimination steps (0.175 (POM s)$^{-1}$) at 343 K, consistent with the deprotonation of the butoxides, also required for double-bond isomerization, occurring much faster than the elimination steps that form the butoxides during dehydration.[12] DFT calculations confirm the kinetic relevance of elimination steps and the low concentrations of adsorbed butoxides. Butene desorption (88 kJ mol^{-1}) barriers are lower than the E1-type elimination barriers (132 kJ mol^{-1}) by 44 kJ mol^{-1}. In addition, the barrier for concerted desorption of H_2O and butene (61.5 kJ mol^{-1}) is also much lower than for C−O and C−H bond breaking occurring in a single step (139 kJ mol^{-1}).[10,13]

cis-/trans-2-Butene isomer ratios are similar for 2-butanol and 1-butanol dehydration, *sec*-butyl-methyl ether cleavage, and 1-butene double-bond isomerization (in the absence of alkanol and ether reactants) (extrapolated to low conversions for the latter) (Figure 3). These ratios (0.95−0.98) are much higher than expected from the thermodynamic stability of these isomers (0.4, 343 K). For elimination reactions, cis/trans isomer ratios are independent of residence time, indicating that they reflect the stereospecificity imposed by the steps that form alkenes during elimination catalytic cycles. The similar cis/trans isomer ratios given by all reactants suggest that *sec*-butoxy intermediates are involved in selectivity-controlling desorption steps for all reactants (Figure 3). The *cis-/trans*-2-butene selectivity ratio depends on the relative energies and the ratios of the partition functions of the different stereoisomeric intermediates (adsorbed alkanol monomers for E2 and alkoxides for E1-type pathways) and transition states of the C−H bond-breaking step as double bonds incipiently form and rotation can no longer occur (see Supporting Information for the scheme). The low rotational barriers[14] involved are consistent with quasi-equilibrated adsorbed stereoisomers and cis/trans ratios thus reflect only the ratios of the partition functions and the energy differences in their respective transition states (see Supporting Information for the derivation); they are insensitive, however, to the nature of the intermediates preceding the transition state in which the double bond is formed. The inference that similar cis/trans ratios reflect common *sec*-butoxy intermediates requires that the relative free energies for cis and trans transition states be different for E1 and E2 elimination pathways. The different transition-state structures of the three (1-butanol, 2-butanol, and *sec*-butyl-methyl ether) different C_4 reactants in E2 elimination make similar cis/trans ratios for elimination and isomerization unexpected when elimination avoids the formation of butoxide intermediates and their deprotonation, as in the case of E2 mechanisms.

H-D kinetic isotope effects (KIE) can discern otherwise unavailable features of the breaking, making, and rehybridization of C−H or O−H bonds. If reaction coordinates involve proton transfer, $O_{cat}\rightarrow H \rightarrow O_{alkanol}$ in E1 or E2 transition states (Chart 1a,b) or $C_\beta\rightarrow H\rightarrow O_{cat}$ in E2 transition states (Chart 1b), $\nu_{Ocat\text{-}H}$

(12) We note that both rate constants reflect the saturation coverage of either butoxides in 1-butene double bond isomerization or adsorbed butanol monomers in 2-butanol dehydration and allow rigorous conclusions with respect to the kinetic relevance of the butoxide desorption and the elimination step.

(13) The high pre-exponential factor of the elimination step leads to rate constants for the elimination and butene desorption steps that differ less than expected from the calculated barriers (see also section 3.2).

(14) The rotational barriers for the interconversion of the different stereoisomers are low (~10 to 15 kJ mol^{-1}) Anslyn, E. V.; Dougherty, D. A. *Modern Physical Organic Chemistry*; University Science Books: New York, 2006; p 93.

Chart 1. Proposed Transition States Involving Proton Transfer That Would Lead to High Kinetic Isotope Effects in E1 (a) and E2 (b) Elimination Steps

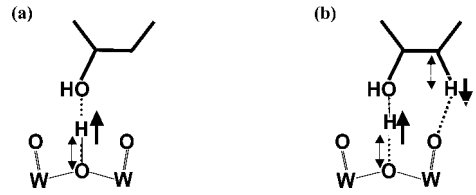

Table 2. Rate and Equilibrium Constants k_2 and K_4 (Scheme 1) for Various Alkanol and Ether Molecules at 343 K on $0.04H_3PW/SiO_2$

reactant	k_2 (10^{-3} (H^+ s)$^{-1}$)	K_4 (kPa^{-1})
2-butanol	60	21
1-butanol	0.09	91
1-butanol-d_{10}	0.07	70
tert-butanol	3300	0.3
2-propanol-d_0	12	8
2-propanol-d_8	8	9
2-propanol-d_6[a]	7	8
sec-butyl-methyl ether	10	1.5

[a] CD_3-CHOH-CD_3.

and $\nu_{C\beta\text{-}H}$ stretching modes become proton translations (and acquire an imaginary frequency), and these translations do not contribute to the zero-point vibrational energies (ZPVE) of activated complexes; in such cases, KIE values of $\gg 10$ are expected at 343 K.[15] Smaller isotope effects do not unequivocally reject relevant X-H(D) activation steps, because late or early transition states can contain intact or cleaved X−H(D) bonds, respectively, which lead, in turn, to small ZPVE effects.

KIE values measured for the elimination rate constant (k_2) in dehydration of 2-propanol-d_0 and 2-propanol-d_8 were small ($(k_{2,H}/k_{2,D}) = 1.4$ at 343 K for $H_3PW_{12}O_{40}$) and thermodynamic isotope effects for dimer formation (K_4) were near unity ($K_{4,H}/K_{4,D} = 0.9$) (Table 2). These isotope effects are much smaller than reported previously for 2-butanol ($CD_3CD_2CH(OH)CD_3$) dehydration on γ-Al_2O_3 (4.1 at 403 K),[16] which were taken as evidence for E_2-type pathways. Similarly, small isotope effects were also observed for 1-butanol-d_{10} dehydration (Table 2). The small KIE values measured here on POM clusters are inconsistent with $C_\beta \rightarrow H \rightarrow O_{cat}$ proton transfer (Chart 1b) in E2 transition states or with $O_{cat} \rightarrow H \rightarrow O_{alkanol}$ proton transfer in E1 and E2 transition states (Chart 1a,b). They indicate instead that $O_{cat}-H$ bonds are cleaved and $H-O_{alkanol}$ bonds are formed in the transition state, a conclusion consistent with the late transition-state structures identified for both E1 and concerted C−O and C−H bond-breaking elimination pathways by density functional theory calculations[4,10] and with the strong effect of carbenium ion stability on elimination rate constants, discussed in section 3.2. KIE values for $CD_3-CHOH-CD_3$ (1.6 at 343 K) and $CD_3-CDOD-CD_3$ (1.4) were similar. If $C_\alpha-H_\alpha$ bond rehybridization, which affects $C_\alpha-H_\alpha$ out-of-plane bending vibrations,[17] accounted for isotope effects with $CD_3-CDOD-CD_3$, then $CD_3-CHOH-CD_3$ would have given KIE values (with respect to $CH_3-CHOH-CH_3$) of unity, because $C_\alpha-H_\alpha$ bonds in $CD_3-CHOH-CD_3$ contain only protium. Measured KIE values reflect a transition state in which the number of C−H(D) and O−H(D) bonds is the same as for the preceding reactive intermediate, a condition met by the late carbenium-ion-type transition state identified for E1 2-butanol dehydration pathways.[10] Proton-transfer, a widely studied process,[18] is required for elimination reactions catalyzed by acids, but its dynamics and energetics do not control elimination rates or barriers. We discuss later the properties of the catalyst and of the reactants critical to the stability of the transition states in the kinetically relevant elementary step.

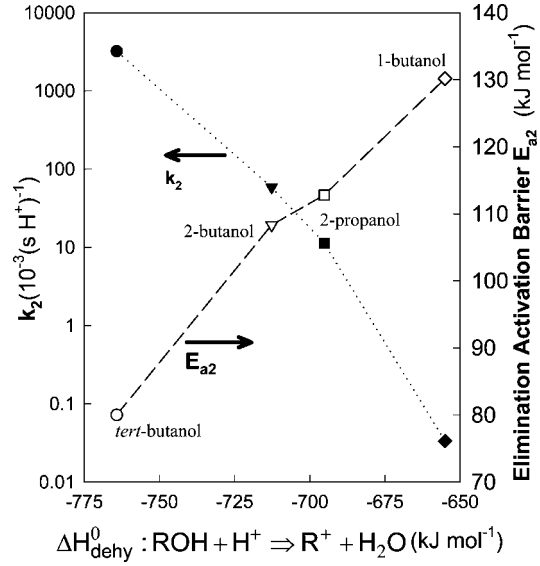

Figure 4. Values of k_2 (full symbols) and E_{a2} (open symbols) as a function of dehydration enthalpy ΔH^0_{dehy} for: ROH + $H^+ \rightarrow R^+ + H_2O$ (eq 4) (see also Chart 2b) for *tert*-butanol (●), 2-butanol (▼), 2-propanol (■), and 1-butanol (♦) (0.04 H_3PW/Si, (343 K (k_2), 333 − 373 K (E_{a2})).

3.2. Implications of the Late Carbenium-Ion Type Transition State on Elimination Rate Constants. Next, we probe substituent effects at C_α-centers in alkanols using 1-butanol, 2-butanol, *tert*-butanol, and 2-propanol as reactants to examine the nature of the elimination transition states and the transition state energies with thermochemical cycles. The k_2 values increased exponentially (k_2 (1-butanol) $\ll k_2$ (2-propanol) $< k_2$ (2-butanol) $\ll k_2$ (*tert*-butanol)) (Figure 4), while elimination activation energies (E_{a2}, Figure 4) decreased linearly as the enthalpy[19–21] for the formation of R^+ and H_2O in gas phase dehydration reactions (ΔH^0_{dehy}(eq 4)) becomes more negative with increasing substitution at C_α-centers

$$ROH + H^+ \Rightarrow R^+ + H_2O\ \Delta H^0_{dehy} \qquad (4)$$

and as the cationic product (R^+, carbenium ion) becomes concurrently more stable relative to its alkanol precursor and the proton.

(15) The difference in νO-H and νO-D stretching vibrations is estimated to be about 700 cm^{-1} for 2-propanol-d_0 and 2-propanol-d_8 H-bonded to H_2SO_4 by DFT, corresponding to zero point energy differences ΔZPE(D)−ZPE(H) of about 8.3 kJ/mol, leading to a KIE of 18.8.

(16) Knözinger, H.; Scheglila, A. *J. Catal.* **1970**, *17*, 252. ("the high isotope effects which result from deuteration in α-position imply a rate-determining participation of the Cα-H(D) bond fission during the dehydration course")

(17) Anslyn, E. V.; Dougherty, D. A. *Modern Physical Organic Chemistry*; University Science Books: New York, 2006; p 429.

(18) (a) Hynes, J. T.; Klinman, J. P.; Limbach, H.-H.; Schowen, R. L. *Hydrogen Transfer Reactions*, Wiley-VCH: Weinheim, Germany, 2007. (b) Mohammed, O. F.; Pines, D.; Dreyer, E.; Pines, E.; Nibbering, E. T. *Science* **2005**, *310*, 83–86. (c) Eigen, M. *Angew. Chem. Int. Ed.* **1964**, *2*, 285.

(19) Aue, D. H.; Bowers, M. T. *Gas Phase Ion Chemistry*; Academic Press: New York, 1970: Vol. 2, p 32.

(20) Stull, D. R.; Westrum, E. F.; Sinke, G. C. *The Chemical Thermodynamics of Organic Compounds*; Wiley: New York, 1987.

(21) Hunter, E. P. L.; Lias, S. G. *J. Phys. Chem. Ref. Data* **1998**, *27*, 413.

Chart 2. Thermochemical Cycles for Acid−Base Reactions over POM Acid Catalysts for Early (a) and Late (b) Transition States

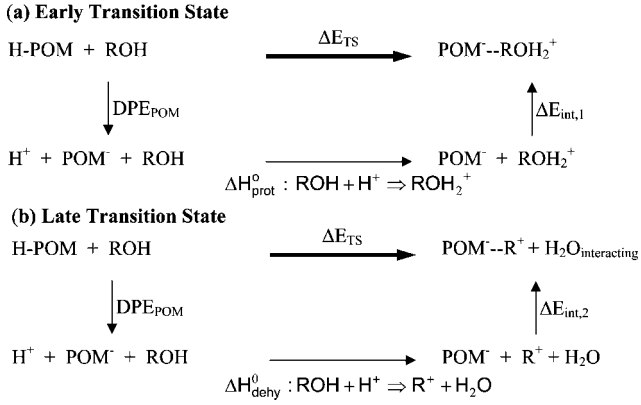

The effects of R^+ stability and ΔH^0_{dehy} on elimination rate constants and activation barriers can be interpreted using thermochemical cycles, introduced first in the context of Brønsted acid catalysis by Gorte and co-workers,[22] that form the proposed elimination transition states (Chart 2). The energy of the transition state (ΔE_{TS}; relative to the reactants in the gas-phase and the free POM cluster) is:

$$\Delta E_{TS} = DPE + \Delta H_{rxn} + \Delta E_{int} \quad (5)$$

where DPE is the deprotonation enthalpy (endothermic) of the POM cluster:

$$HPOM \rightarrow H^+ + POM^- \qquad DPE = \Delta H \quad (6)$$

which depends, in turn, on the H−POM dissociation energy, the electron affinity of the POM• cluster, and the ionization energy of H atoms. ΔH_{rxn} is either the enthalpy for protonation

$$ROH + H^+ \Rightarrow ROH_2^+ \qquad \Delta H^0_{prot} \quad (7)$$

(exothermic) (Chart 2a), the appropriate measure for early dehydration transition states, or the enthalpy for dehydration (eq 4) (exothermic) (Chart 2b), appropriate for a late dehydration transition state. Both terms include the enthalpy for O−H bond formation, the ROH (early TS) or R (late TS) ionization energies, and the electron affinity of H^+. Typical DPE values for Brønsted acids are 1080 kJ mol^{-1} for H_3PW,[4] a very strong acid, 1171−1200 kJ mol^{-1} for zeolites,[23] 1293 kJ mol^{-1} for H_2SO_4,[24] and 1600 kJ mol^{-1} for H_2O,[24] a very weak acid. ΔH_{prot} values vary from −540.5 kJ mol^{-1} (CO_2) to −930 kJ mol^{-1} (pyridine). Values of ΔH_{prot}[21] are readily available, but DPE values are accessible only through theoretical estimates. For POM clusters, these estimates cannot be compared with experimental data, but calculations for small molecules, for which data are available, indicate that DFT methods underestimate DPE values by ∼2%.[10] The ΔE_{int} term (a negative value) in eq 5 represents the interaction energy of $ROH_2^+\cdots POM^-$ ion-pair (for early transition states) or of the $(H_2O)R^+\cdots POM^-$ ion-pair (for late transition states).[25] For ionic transition states, Coulombic stabilization is the predominant contribution to this interaction energy.

The activation barrier for E1 elimination (E_{a2}) reflects the energy difference between reactants and transition states:

$$E_{a2} = \Delta E_{TS} - \Delta H_{ads,ROHmonomer} \quad (8)$$

where $\Delta H_{ads,ROHmonomer}$ is the enthalpy of adsorption for the monomer,

$$ROH + HPOM \Rightarrow ROH\text{-}HPOM \qquad \Delta H_{ads,ROHmonomer} \text{ (cf. step 1, Scheme 1)} \quad (9)$$

For a given POM composition, activation barriers for different ROH reactants change because of differences in (i) ΔH_{rxn}, (ii) ΔE_{int}, and (iii) $\Delta H_{ads,ROHmonomer}$ (eqs 5 and 8). Late cationic transition states would be very sensitive to the extent of substitution in the ROH backbone, because of strong effects on the stability of R^+ species (eq 4), which are reflected in ΔH_{rxn}. The ΔE_{int} values are less sensitive to substitution, because the distance between the positive C_α-atom and the anion determines, for the most part, the Coulombic effects in ΔE_{int}, and are expected to decrease as ΔH_{rxn} becomes more negative and R^+ becomes more stable, because a more substituted and stable R^+ species leads to a more delocalized charge around the α-carbon.[26] Thus, the ΔE_{int} term attenuates the effects of ROH substitution on E_{a2} (eqs 5 and 8) predicted from gas-phase stabilities. $\Delta H_{ads,ROHmonomer}$ values from DFT vary by <10 kJ/mol among ROH species (−70.3 kJ/mol^{-1} (*tert*-butanol) to −76.9 kJ mol^{-1} (2-butanol)),[10,27] suggesting that differences in E_{a2} for various ROH reactants reflect predominantly ΔH_{rxn} effects, albeit attenuated by concomitant effects of substitution on ΔE_{int}.

The difference in stability (ΔH^0_{prot} (eq 7))[21] between protonated *tert*-butanol and 1-butanol (from gas-phase ion−molecule thermodynamic data) is only −13.4 kJ mol^{-1}, while measured activation energies for their elimination reactions differ by 50 kJ mol^{-1} (Figure 4 and Figure S2 (Supporting Information)). Differences in ΔH^0_{dehy} (eq 4) between *tert*-butanol and 1-butanol are, however, much larger (−138.7 kJ mol^{-1}).[19−21] As a result, early transition states would give weak effects of alkanol substitution on k_2 and E_{a2}, reflecting the minor differences in stability for various protonated alkanols. The strong effects of ΔH^0_{dehy} on rates and their linear correlation with elimination barriers (Figures 4 and S2) are consistent with "carbenium-type" late elimination transition states. Differences in E_{a2} are smaller than in ΔH^0_{dehy} because of compensation of the effects of ΔH^0_{dehy} by concomitant changes in ΔE_{int}. The ΔH^0_{dehy} (eq 4) values are less negative than those for ΔH^0_{prot} (eq 7) (Figure S2). Thus, the energy of a "hypothetical" early transition state is, according to eq 5, lower than the energy of a "hypothetical" late transition state. We conclude, therefore, that the transition state occurs late along the reaction coordinate. The late character of the elimination transition state, already evident from the stability of ROH_2^+ gas phase moieties, is consistent with DFT estimates[4,10] and with the small measured kinetic isotope effects, which confirm the kinetic irrelevance of proton transfer at the relevant transition state.

1-Butanol reacts with the smallest rate constant (k_2) and the highest activation barrier among alkanol reactants. The 1-butene/2-butene (*cis*- and *trans*-2-butene) ratios are above equilibrium values (0.24 vs 0.04) and independent of residence time. The preferred formation of 2-butene reflects facile hydride transfer

(22) Aronson, M. T.; Gorte, R. J.; Farneth, W. E. *J. Catal.* **1986**, *98*, 434.
(23) Brändle, M.; Sauer, J. *J. Am. Chem. Soc.* **1998**, *120*, 1556.
(24) Koppel, I. A.; Burk, P.; Koppel, I.; Leito, I.; Sonoda, T.; Mishima, M. *J. Am. Chem. Soc.* **2000**, *122*, 5114.
(25) The ΔE_{int} term of the late transition state ($(H_2O)R^+\cdots POM^-$) ion-pair also includes the stabilizing $R^+\cdots H_2O$ (ion-dipole) interaction.
(26) Robbins, A. D.; Jin, P.; Brinck, F.; Murray, J. S.; Politzer, P. *Int. J. Quantum Chem.* **2006**, *106*, 2904.
(27) Janik, M. J.; Davis, R. J.; Neurock, M. *Catal. Today* **2005**, *105*, 134.

during elimination steps that form *sec*-butoxy intermediates and a carbenium-ion type transition state. Desorption of the primary butoxide via concerted steps involved in alkoxide desorption[27,28] or in concerted E2 elimination steps cannot form 2-butenes. Hydride transfer during E1 elimination steps accounts for the isomers formed.

Thus, we conclude that E1 pathways involving late transition states with significant carbenium-ion character prevail in alkanol dehydration and ether cleavage reactions catalyzed by POM clusters. These late transition states lead to substantial entropy gains in decomposition reactions as six vibrational modes are incipiently converted into three translational and rotational degrees of freedom.[29] These large and positive activation entropies are evident in the large pre-exponential factors measured for the kinetically relevant elimination steps in 2-butanol dehydration reactions ($1.5-1.9 \times 10^{15}$ s^{-1} for 2-butanol dehydration on $H_{8-n}X^{n+}W$ (X = P, Si, Al), Table S1 (see Supporting Information)). These values are more than 100 times larger than predicted if the chemisorbed butanol reactants and the E1 transition state had similar entropies ($\sim 10^{13}$ s^{-1}) and correspond to a gain in entropy of $\sim$40 J $(mol\ K)^{-1}$. In contrast, the concerted transition states required for E2 elimination pathways exhibit a highly ordered structure (Chart 1b), with significantly lower entropies than chemisorbed butanol reactants and would lead to low values of the pre-exponential factors ($<10^{13}$ s^{-1}).[29] The high pre-exponential factors measured for 2-butanol dehydration (and also for 1-butanol, *tert*-butanol, 2-propanol, and sec-butyl-methyl ether) are consistent with the prevalence of E1 decomposition pathways in alkanol dehydration and ether cleavage reactions. The low temperatures required for alkanol dehydration catalysis reflect the high entropy, instead of the low energy, of the relevant transition state.

3.3. Inhibition of Alkanol Dehydration and Ether Cleavage by *n*-Donors. We discuss next the effects of H_2O and of alkanol and ether reactants on the nature and stability of adsorbed species and on their reactivity in elimination reactions. Figure 5 shows that inverse 2-butanol dehydration rates are proportional to 2-butanol pressures, but also to the combined pressures of 2-butanol and H_2O on $0.04H_3PW/Si$ and $0.04H_5AlW/Si$. Thus, the inhibition effects of H_2O and 2-butanol are similar in magnitude, even though they can reflect coadsorbed H_2O monomers (K_6 equilibrium constant), H_2O dimers (K_7), or mixed 2-butanol/H_2O dimers (K_5), as well as unreactive butanol dimers (K_4), the combined effects of which lead to dehydration rates given by

$$r = \frac{k_2K_1[C_4H_9OH][H^+]}{1 + K_1[C_4H_9OH] + K_1K_4[C_4H_9OH]^2 + K_1K_5[C_4H_9OH][H_2O] + K_6[H_2O] + K_6K_7[H_2O]^2} \quad (10)$$

in which the denominator terms reflect the relative concentrations of H^+, 2-butanol monomers and dimers, mixed 2-butanol-H_2O dimers, and H_2O monomers and dimers in the sequence in which they appear. The measured trends (Figure 5) indicate that K_4 and K_5 have similar values and that terms not containing K_1 are much smaller, which results in a form of eq 10 consistent with the data in Figure 5:

$$r^{-1} = \frac{1}{k_2[H^+]} + \frac{K_4}{k_2[H^+]}([C_4H_9OH] + [H_2O]) \quad (11)$$

The dimer formation enthalpies estimated from DFT for interactions of adsorbed butanol with H_2O (-79.7 kJ mol^{-1}) or with another butanol (-83.7 kJ mol^{-1})[10] are similar. This is an unexpected finding because $R_1O-H^+\cdots OR_2$ hydrogen bonding is expected to strengthen as the proton affinities of R_1O and R_2O become similar, as is the case for butanol dimers. In contrast, the proton affinity ($PA = -\Delta H^0_{prot}$) for 2-butanol (793.7 kJ mol^{-1}) is much higher than for H_2O (691 kJ mol^{-1}).[21] The stability of $ROH^+\cdots OH_2$ species, given by the hydrogen bond dissociation energy (ΔH^0_D) can be estimated from correlations between bond dissociation energies and proton affinity differences (ΔPA):[30]

$$\Delta H^0_D(ROH^+\cdots OH_2) = 127.3 - 0.3\Delta PA \quad (12)$$

This equation predicts a significant decrease in ΔH^0_D from 127.3 kJ mol^{-1} for 2-butanol dimers to 96.5 kJ mol^{-1} for 2-butanol/H_2O dimers. It appears that steric repulsion between synperiplanar *sec*-butyl groups causes 2-butanol dimers coordinated to Keggin anions to be less stable than expected from their antiperiplanar structure as gaseous dimers (Chart 3); these steric repulsion effects are much weaker for coordinated butanol-

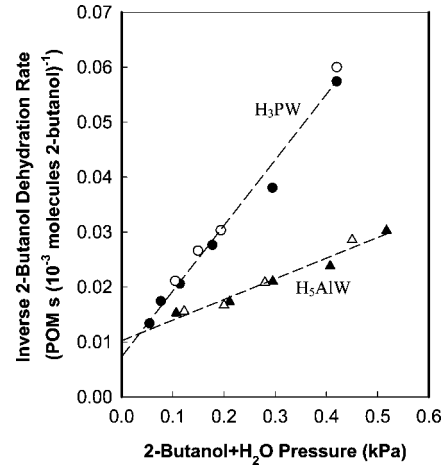

Figure 5. Inverse 2-butanol dehydration rates (per POM) at 343 K as a function of 2-butanol pressure (full symbols) and the sum of 2-butanol and H_2O pressures on $0.04H_3PW/Si$ (●/○) and $0.04H_5AlW/Si$ (▲/△). Open symbols show inverse rates as a function of 2-butanol/H_2O pressures, full symbols show inverse rates for different 2-butanol pressures.

Chart 3. Syn- (a) and Antiperiplanar (b) Protonated 2-Butanol Dimer

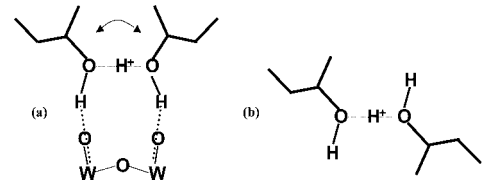

(28) The transition state of alkene desorption on POM clusters has been shown to be concerted and to involve both a weak interaction of C_α (which carries the positive charge) with a terminal oxygen of the POM cluster and the interaction of a β-H with the bridging oxygen of the POM cluster. Abstraction of the β-H and formation of the alkene double bond will lead to the formation of the 1-alkene species. Campbell, K. A.; Janik, M. J.; Neurock, M.; Davis, R. J. *Langmuir* **2004**, *21*, 4738.

(29) Benson, S. W. *Thermochemical Kinetics*; Wiley: New York, 1976.

(30) Meot-Ner (Mautner) , M. *J. Am. Chem. Soc.* **1984**, *106*, 1257.

H_2O dimers. DFT estimates gave H_2O adsorption ($H_2O\cdots H_3PW$) enthalpies of -67.6 kJ mol^{-1},[27] which are less negative than for 2-butanol adsorption (-76.9 kJ mol^{-1}),[10] in agreement with rate data indicating that K_1 is larger than K_6.

2-Butanol dehydration turnover rates (0.1 kPa 2-butanol) measured in the presence of added H_2O (0.1−0.4 kPa) were higher on H_5AlW/SiO_2 than on H_3PW/SiO_2, even though the former has a higher deprotonation enthalpy and a lower acid strength (Figure 5).[4] These trends, unexpected at first glance, reflect dehydration rates that depend on $(k_2[H^+])/K_4$ (eqs 2 and 11) at high 2-butanol (Figures 1 and 2) or combined 2-butanol and H_2O pressures (Figure 5).

We conclude that $(k_2[H^+])/K_4$ terms determine the kinetic tolerance of a given acid to the presence of water and other *n*-donors. Kinetic inhibition of elimination reactions by water is not caused by competitive adsorption—the concentration of H_2O monomers and dimers is low—but by mixed 2-butanol-H_2O dimers, in which H_2O solvates the predominant reactive intermediates (alkanol monomers). These effects and their sensitivity to the identity and strength of the acid were not considered in a recent review[31] of water-tolerant solid acid catalysts, which proposed surface hydrophobicity as the relevant criterion for water tolerance. Below, we discuss, using thermochemical cycles, the origin of the inhibition by *n*-donor molecules, such as water products or alkanol reactants and its dependence on the identity of the acid and the active site.

Thermochemical cycles relevant for estimates of k_2 and K_4 indicate that k_2/K_4 ratios are independent of deprotonation enthalpy (or acid strength):

$$\frac{k_2}{K_4} = \frac{A_2 \exp\left(-\frac{E_{a2}}{RT}\right)}{A_4 \exp\left(-\frac{\Delta H_{dim}}{RT}\right)} = \frac{A_2 \exp\left(-\frac{DPE + \Delta H^0_{dehy} + \Delta E_{int,2} - \Delta H_{ads,ROHman}}{RT}\right)}{A_4 \exp\left(-\frac{DPE + \Delta H^0_{dim} + \Delta E_{int,4} + \Delta H_{ads,ROHman}}{RT}\right)} = \frac{A_2}{A_4} \exp\left(-\frac{(\Delta H^0_{dehy} - \Delta H^0_{dim}) + (\Delta E_{int,2} - + \Delta E_{int,4})}{RT}\right) \quad (13)$$

A_2 and A_4 are pre-exponential factors for elimination and dimer formation steps, respectively. ΔH_{dim} is the dimer formation energy. $\Delta E_{int,2}$ is the interaction energy of R^+ and H_2O with deprotonated POM clusters in the elimination transition state and $\Delta E_{int,4}$ is the interaction energy of protonated 2-butanol dimers or 2-butanol−H_2O dimers with deprotonated anionic POM clusters. ΔH^0_{dim} is the enthalpy of formation of the respective gas phase dimers:

$$R_1OH + R_2OH + H^+ \Rightarrow (R_1OH)H^+(R_2OH) \qquad \Delta H^0_{dim} \quad (14a)$$

$$\Delta H^0_{dim} = \Delta H^0_{prot}\ (\text{eq } 7) + \Delta H^0_D\ (\text{eq } 12) \quad (14b)$$

A_2 and A_4 are nearly independent of the identity of the central atom (see Table S1 (Supporting Information)) and the different k_2/K_4 ratios on H_5AlW and H_3PW therefore reflect the effects of E_{a2} and ΔH_{dim} (eq 13). The effects of the central atom on ΔH_{dim} are stronger than on E_{a2} (see Table S1 (Supporting Information)). These thermochemical cycles together with experimental data for E_{a2} and ΔH_{dim} and the calculated DPE and experimental (gas-phase ion-chemistry) ΔH_{rxn} values allow estimates for $\Delta E_{int,2}$ and $\Delta E_{int,4}$. The $\Delta E_{int,4}$ values are less negative and increase more weakly with decreasing valence of the central atom than the values for $\Delta E_{int,2}$ (Table 3). The less negative $\Delta E_{int,4}$ values and smaller differences in $\Delta E_{int,4}$ values among $H_{8-n}X^{n+}W_{12}$ clusters with different central atoms for the dimer species compared to the $\Delta E_{int,2}$ values appear to reflect a smaller positive charge in the dimer species or a larger charge separation of the dimer and the anionic conjugate base than for the carbenium ion transition states (to be discussed in detail in section 3.4).[32]

Table 3. Deprotonation Enthalpies (DPE) (eq 6), 2-Butanol Monomer Adsorption Enthalpies $H_{ads,mon}$ (eq 9), Gas-Phase Dehydration Enthalpies (ΔH^0_{dehy}) (eq 4), Gas-Phase Dimer Formation Enthalpies (ΔH^0_{dim}) (eq 14b), and Interaction Energies ($E_{int,2}$ and $E_{int,4}$) on $0.04H_{8-n}X^{n+}W/SiO_2$ (where X= P, Si, Al) (See Also Chart 2)

(kJ mol^{-1})	DPE[a]	$\Delta H_{ads,mon}$[a]	$\Delta H_{rxn,2}$[b]	$E_{int,2}$[c]	$\Delta H_{rxn,4}$[d]	$E_{int,4}$[e]
$0.04H_3PW/SiO_2$	1087	−76.9	−713	−43	−930	−303
$0.04H_4SiW/SiO_2$	1105	−75.8	−713	−358	−930	−316
$0.04H_5AlW/SiO_2$	1121	−72.8	−713	−370	−930	−326

[a] DFT results (cf. refs 4 and 10). [b] cf. eq 4. $H_{rxn,2} = H^0_f$ (sec butyl carbenium ion, ref 19) (766 kJ mol^{-1}) + H^0_f (H_2O, ref 20) (−241.8 kJ mol^{-1}) − H^0_f (H^+, ref 19) (1530 kJ mol^{-1}) − H^0_f (2-butanol, ref 20) (−293 kJ mol^{-1}) kJ mol^{-1}. [c] cf. eq 16, $E_{int,2} = E_{a2}$ (Table S1) − DPE − $H_{rxn,2}$ + $H_{ads,mon}$. [d] H_{prot} (eq 7) (2-butanol, ref 21) (−793 kJ mol^{-1}) + H^0_D (eq 12, ref 30). (−127.3 kJ mol^{-1}). [e] $E_{int,4} = H_{dim}$ (Table S1) − DPE − $H_{rxn,4}$ + $H_{ads,mon}$.

Turnover rates for 1-butanol, 2-butanol (Figure 1), *tert*-butanol, and 2-propanol dehydration and for *sec*-butyl-methyl ether elimination (Figure 1) showed similar kinetic dependence on reactants. All data are described accurately by eq 2. Thus, inhibition reflects the stability provided by the $[-O\cdot-\cdot H\cdot-\cdot O\cdot-]^+$ hydrogen bond (ΔH^0_D), that leads to the formation of unreactive dimers and a significant decrease (−127.3 kJ/mol^{-1} (eq 12)) in $\Delta H_{dim}{}^0$ (eq 14b),

$$\Delta H_{dim} = DPE + \Delta H^0_{prot} + \Delta H^0_D + \Delta E_{int,4} - \Delta H_{ads,ROHmonomer} < 0 \quad (15)$$

compared to ΔH^0_{prot}. It is the stability gained by the formation of the $[-O\cdot-\cdot H\cdot-\cdot O\cdot-]^+$ hydrogen bond in dimers (ΔH^0_D (eq 12) term in eq 15) that allows proton transfer and the formation of more stable ionic complexes ($\Delta H_{dim} < 0$).[4] $\Delta H_{dim}{}^0$ (eq 14b) (= −PA (2-butanol dimer)) is −913 kJ mol^{-1}, significantly more negative than ΔH^0_{prot} (2-butanol) (−793 kJ mol^{-1}) and comparable to ΔH^0_{prot} (pyridine) (−930 kJ mol^{-1}). Adsorbed 2-butanol is strongly stabilized by solvation with another butanol molecule, but DFT estimates and rate data indicate that such solvation is much less effective for the corresponding elimination transition state, leading to higher activation barriers upon solvation and to inhibition.[10] Inhibition via dimer formation is common for reactions involving *n*-donor reactants, products, or solvents, in either the liquid or the gas phase.

The equilibrium constants (K_4) for dimer formation decreased with increasing substitution in reactants (1-butanol > 2-butanol > 2-propanol > *sec*-butyl-methyl ether > *tert*-butanol) (Table 2), a trend that reverses the ranking of their proton affinities (*sec*-butyl-methyl ether > tert-butanol > 2-propanol ≈ 2-butanol > 1-butanol).[21] These data are consistent with steric destabiliza-

(31) Okuhara, T. *Chem. Rev.* **2002**, *102*, 3641.

(32) Charge transfer from POM^- to the dimer $(ROH)_2H^+$ is indicated by two $O_{alkanol}$-$H_{alkanol}\cdots O_{POM}$ hydrogen bonds between the cationic dimer and the anionic conjugate base [ref 10].

Chart 4. Protonated *tert*-Butanol Dimer (a) and the Mixed Protonated *tert*- and 1-Butanol Dimer (b)[a]

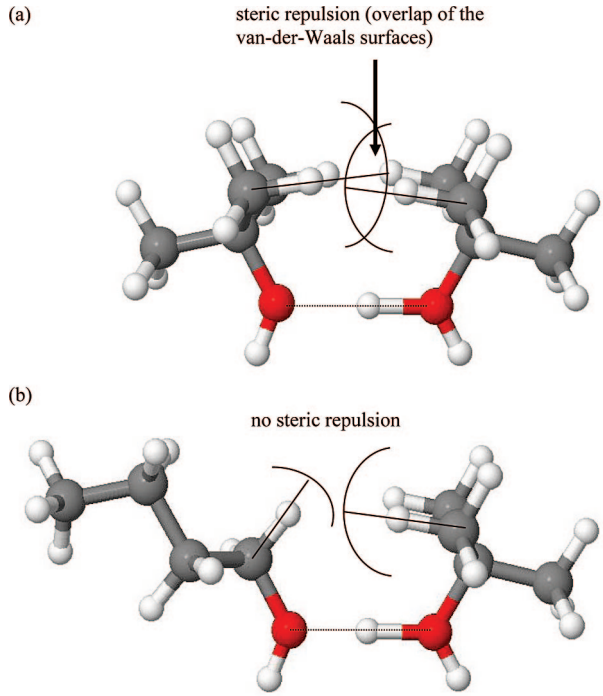

[a] The O—O distance is kept equal for both dimers. For structure a the formation of a strong $(O-H-O)^+$ cationic hydrogen bond is prevented by the steric repulsion of the two *tert*-butyl groups.

tion of dimers for bulkier *tert*-butanol (Chart 4a) and ether reactants. Replacing a $-CH_3$ group at C_α (in 2-butanol) with $-H$ (in 1-butanol) increased K_4 (from 21 to 91.5 kPa^{-1} at 343 K, Table 2), consistent with this proposal. These steric effects are also evident in the stronger inhibition of *tert*-butanol dehydration by coadsorbed H_2O (or coadsorbed 1-butanol) relative to the weak self-inhibition by *tert*-butanol, because less bulky H_2O and 1-butanol molecules solvate adsorbed *tert*-butanol monomers more effectively than another *tert*-butanol. Chart 4a illustrates the stronger steric repulsion in protonated *tert*-butanol dimers relative to *tert*-butanol-1-butanol dimers (Chart 4b) by the overlap of van-der-Waals surfaces of the alkyl groups of the *tert*-butanol monomers for the protonated *tert*-butanol dimer, which is indicative for steric repulsions. *sec*-Butyl-methyl ether dimers may also be destabilized relative to dimers of alkanols or H_2O, because they cannot form two $O_{alkanol}-H_{alkanol}\cdots O_{POM}$ hydrogen bonds; thus, dimer formation becomes less exothermic and inhibition constants (K_4 values) (Table 2) become smaller for *sec*-butyl-methyl ether than for 2-butanol.

3.4. Energies of Cationic Transition States and Intermediates in Terms of Reactant and Catalyst Properties. The activation energy for a step involving cationic transition states can be written as (see section 3.2 and Chart 2)

$$E_a = \mathrm{DPE} + \Delta H_{rxn} + \Delta E_{int} - \Delta H_{ads,ROHmonomer} \qquad (16)$$

where ΔH_{rxn} is the enthalpy for proton transfer ($H^+ + R-X \rightarrow$ product(s)) with or without R—X cleavage to give $R^+ + X-H$ or RXH^+, respectively. Thus, these activation barriers reflect the energy required to move a proton far from the anionic conjugate base minus the energy gained by reacting H^+ with reactants (ΔH_{rxn}) and by allowing protonated reactants or reaction products to interact with the anionic conjugate base

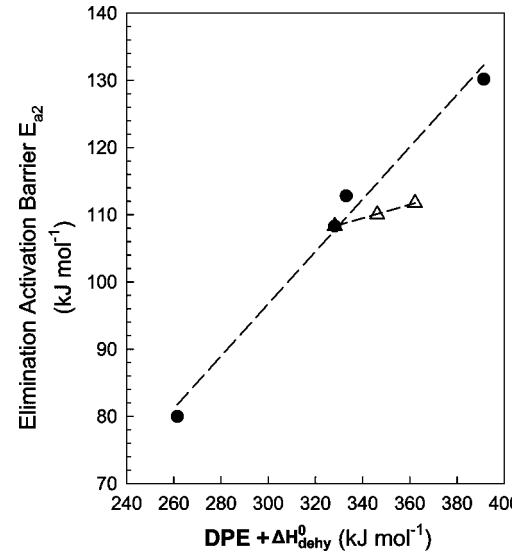

Figure 6. ROH elimination activation barrier E_{a2} (Scheme 1, step 2) as a function of the sum of deprotonation enthalpy (DPE)[4,10] and gas-phase dehydration reaction enthalpy (ΔH^0_{dehy}: $ROH + H^+ \Rightarrow R^+ + H_2O$[19–21] (Chart 2b) for $0.04H_{8-n}X^{n+}W/Si$ (Δ) (X = P, Si, and Al, in the order of increasing DPE) for 2-butanol dehydration, and for $0.04H_3PW/Si$ and different ROH reactants (●) (*tert*-butanol, 2-butanol, 2-propanol, 1-butanol, in the order of increasing ΔH^0_{dehy}) (343 K). Dashed lines represent a fit assuming a linear dependence of E_{a2} and (DPE + ΔH^0_{dehy}).

(ΔE_{int}). Equation 16 indicates that E_a increases (and k_i decreases) with increasing (DPE $+\Delta H_{rxn}$) values. DPE values vary by 56 kJ mol^{-1} (1087−1143 kJ mol^{-1}; P < Si < Al < Co) among POM clusters with different central atoms.[4] The identical Keggin structures of these clusters together with DFT calculations[4,10] suggest that the nature of the transition state is not sensitive to X in $H_{8-n}XW_{12}$.[4] ΔH_{rxn} can be varied over a broader range (130 kJ mol^{-1}; Figure 4) than DPE values by using different alkanol reactants (*tert*-butanol, 2-butanol, 2-propanol, 1-butanol), for which the extent of substitution at C_α-centers strongly influences ΔH^0_{dehy} (eq 4). Our k_2 and E_{a2} data show the expected correlation with increasing DPE + ΔH^0_{dehy} (Figure 6), but their values depend on (DPE + ΔH^0_{dehy}) more sensitively when these energies are varied by changing the stability of the carbenium ion (ΔH^0_{dehy}) than the identity of the POM central atom (DPE).

Equation 16 shows that DPE and ΔH_{rxn} effects on elimination activation barriers and rate constants can be compensated by a concurrent (i) change in $\Delta H_{ads,ROHmonomer}$ (eq 9) or (ii) ΔE_{int} with DPE of POM clusters (eq 16). DFT estimates (Table 3) for $\Delta H_{ads,ROHmonomer}$ show that it increases only slightly with decreasing valence of the central atom ($\Delta H_{ads,ROHmonomer}$: −76.9 kJ mol^{-1} (H_3PW), −72.8 kJ mol^{-1} (H_5AlW)).[10] Thus, the weaker effects of DPE on k_2 and E_{a2} relative to those of ΔH_{rxn} must reflect instead concurrent changes in ΔE_{int}, and specifically a more favorable interaction between R^+ cations and anionic $(H_{8-n-1}X^{n+}W_{12})^{-1}$ clusters with decreasing valence of the central atom. Equation 16, taken together with DPE and $\Delta H_{ads,ROHmonomer}$ values from DFT calculations,[4,10] gas-phase ΔH_{rxn} data, and measured elimination activation energies E_{a2}, allow us to estimate ΔE_{int} values and to assess the effects of DPE on their magnitude (Table 3). These $\Delta E_{int,2}$ estimates for H_4SiW and H_5AlW show a decrease (became more negative) by 15 and 27 kJ mol^{-1} relative to H_3PW, as DPE values concurrently increased by 18 and 33 kJ mol^{-1} (Table 3). A similar compensation was evident from ΔE_{int} values calculated from DFT activation barriers.[10]

Chart 5. Point Charge Model (b) to Illustrate the Effects of Central Atom on the Interaction Energies. Chart 5a Shows the Relation between the Point Charge Model and the Keggin-Type POM Cluster at the Elimination Transition State

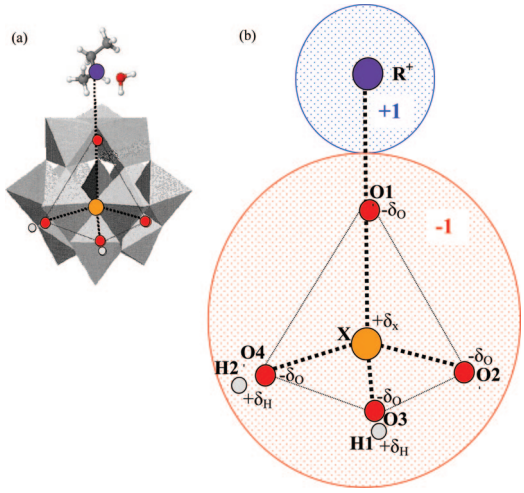

We discuss next the basis for these compensation effects, which lead to more negative ΔE_{int} values at the transition state as DPE values increase and protonated POM clusters become weaker acids. In $H_{8-n}X^{n+}W_{12}O_{40}$ POM clusters, the charge density in the anionic $(H_{7-n}X^{n+}W_{12}O_{40})^{-1}$ shell increases because of the larger number of charge-balancing protons with decreasing valence of X; this leads, in turn, to stronger Coulombic stabilization of the anionic conjugate base−carbenium ion-pair and to the more negative ΔE_{int} values evident from the measurements.

We illustrate these compensation effects with a heuristic construct (Chart 5) that considers a central atom (X) bound tetrahedrally to four negative charges (O_1−O_4) located at the $W_{12}O_{40}$ shell (at a distance of 0.4 nm, corresponding to WO_b−X bonds in Keggin clusters), $(7 - n)$ H atoms at tetrahedral vertices of the shell at a distance of 0.5 nm from X (corresponding to the H−X distances in $H_{8-n}X^{n+}W_{12}O_{40}$ POM clusters), and one positive charge corresponding to the R^+ species located also at a tetrahedral vertex, but 0.7 nm from X (Chart 5) (corresponding to the C_α−X distances in $R^+\cdots(H_{7-n}X^{n+}W_{12}O_{40})^-$ ion-pair at the transition state).[10] The negative charge δ_O on each of the four oxygen atoms (O1−O4) depends on the number (n) and charge (δ_H) of the H atoms, the atomic charge of the central atom δ_X, and the charge on the cationic fragment δ_{R+} (cf. Chart 5):

$$\delta_o = \frac{(\delta_X + n\delta_H - \delta_{R+})}{4} \qquad (17)$$

DFT estimates of Mulliken atomic charges in $H_{7-n}X^{n+}O_4^-$ (X = Cl^{7+}, S^{6+}, P^{5+}, Si^{4+}) show that the charges on the H-atoms are insensitive to the identity of X, that the four O-atoms have similar charges that depend on X, and that the charge on X decreases as its valence increases (see Table S2 (Supporting Information)). As for the O_4 shell in $H_{8-n}X^{n+}O_4$, the charge in the $W_{12}O_{40}$ shell becomes with decreasing valence of X, corresponding to a decrease (more negative) in δ_O in our simple model. The resulting Coulombic interaction energy ($\Delta E_{int,Coul}$) is given by

$$E_{int,Coul} = \sum_i \frac{q_{R+}q_i}{4\pi\varepsilon_0 r_{R+i}} \qquad (18)$$

which gives values (−311 kJ mol^{-1} for XO_4 surrounded by 2 protons, −345 kJ mol^{-1} for 3 protons) very similar to those estimated from measured activation energies with DPE and $\Delta H_{ads,ROHmonomer}$ values from DFT[4,10] and gas-phase ΔH_{rxn} data (−343 kJ mol^{-1} for H_3PW and −358 kJ mol$^-$ for H_4SiW, Table 3). The predictions from eq 18 also follow trends with decreasing valence of X and increasing number of charge balancing protons similar to those observed (e.g., a decrease by 34 kJ mol^{-1} (model), vs 15 kJ mol^{-1} (experiment) in ΔE_{int} (Table 3) for H_3PW and H_5AlW). Similarly, interaction energies from DFT simulations[33] for Na^+ cations with $(H_{7-n}X^{n+}O_4)^-$ (X = Cl^{7+}, S^{6+}, P^{5+}, Si^{4+}) also increase as the valence of X decreases (Table S2, Supporting Information). All three systems (the model structure, $H_{8-n}X^{n+}O_4$, and $H_{8-n}X^{n+}W_{12}O_{40}$) form more stable ion-pairs relative to the noninteracting anion and cation pair as the valence of X decreases, because the increase in charge density on the shell with increasing number of charge balancing protons leads to more favorable Coulombic interactions between cationic transition states or intermediates and anionic clusters. These effects of charge distribution are not accounted for in the magnitude of DPE values, because these values reflect the stability of the anionic conjugate base at an infinite distance from H^+. We suggest that these ion-pair electrostatic effects also account for the weaker effects of X on ΔE_{int} for dimers ($\Delta E_{int,4}$) than on elimination transition states ($\Delta E_{int,2}$) (Table 3). A lower charge in dimers relative to transition states or a larger distance between the cationic dimer fragment and the anionic conjugate base dampen the effects of X on $\Delta E_{int,Coul}$ by decreasing $\Delta E_{int,Coul}$ differences among different $H_{8-n}X^{n+}W_{12}O_{40}$ clusters.[32] Our heuristic construct (Chart 5) indicates that a decrease in R^+ charge from +1 to +0.9 and an increase in the X−R^+ distance by 0.01 nm causes $\Delta E_{int,Coul}$ differences between $H_2XO_4^-$ and $H_3XO_4^-$ to decrease by 4 or 3.7 kJ mol^{-1}, respectively. The experimental differences between H_3PW and H_4SiW are −2 kJ mol^{-1} (($\Delta E_{int,4}$(H_3PW) − $\Delta E_{int,4}$(H_4SiW) − ($\Delta E_{int,2}$(H_3PW) − $\Delta E_{int,2}$(H_4SiW)) for 2-butanol dimers (Table 3). It appears that the increase of the $k_2[H^+]/K_4$ terms with decreasing valence of X in $H_{8-n}X^{n+}W_{12}O_{40}$ POM clusters, which determines the kinetic tolerance of a given acid to the presence of water and other n-donors (cf. section 3.3), depends on subtle differences in the mainly electrostatic stabilization of the cationic transition state (k_2) and intermediate (K_4) by the anionic conjugate base.

The stability of cationic intermediates and transition states depends on both DPE (acid strength) and ΔE_{int}, which is shown here to become more negative with increasing DPE for $H_{8-n}X^{n+}W_{12}O_{40}$ POM clusters and $H_{8-n}X^{n+}O_4^-$ acids (i.e., weak acids lead to strongly interacting ion-pairs). The identity of a given acid affects both DPE and ΔE_{int}, and the later depends also on the transition state or intermediate of interest. The acid that exhibits the lowest barrier for a certain acid-catalyzed reaction step is the one that minimizes the sum of (DPE + ΔE_{int}), which may not always be the strongest acid (if the increase in DPE is more than compensated for by a decrease in ΔE_{int} (more exothermic)). Product selectivities resulting from acid catalyzed reaction pathways or from the kinetic tolerance of a given acid to water or other n-donors do not depend on DPE, but on the difference of ΔE_{int} for the relevant transition states (cf. eq 13). Typically, the stronger acid possesses a larger

(33) The interaction energy ΔE_{int} is estimated as the energy difference of the interacting ion-pair and of the isolated anion $(H_{7-n}X_{n+}O_4)^-$ and cation (Na^+) (ΔE_{int}= $E((H_{7-n}X_{n+}O_4)^-\cdots Na^+)$− $E((H_{7-n}X_{n+}O_4)^-$− $E(Na^+)$).

anion and/or a lower charge density leading to less negative values of ΔE_{int}. This lower charge density, in turn, leads to a lower sensitivity upon the extent of charge separation at the transition state. Thus, weaker acids lead to a higher selectivity for the reaction requiring the least charge separation. The energies of cationic transition states and intermediates ubiquitous in reactions catalyzed by Brønsted acid sites can, to quite some extent, be understood based on the DPE of the acid, the protonation enthalpies of reactants or products (ΔH_{rxn}), and their stabilization energies (ΔE_{int}), which depend most sensitively on the charge density and distribution within the cationic and anionic fragments. These energies predominantly depend on the properties of isolated ionic fragments, a fact that markedly simplifies the rational design of Brønsted acids for catalyzed reactions.

4. Conclusions

Substituent effects clearly show that alkanol dehydration reactions on Keggin-type polyoxometalate clusters involve late carbenium-ion-type transition states in the kinetically relevant elimination step. Similar *cis-/trans*-2-butene selectivity ratios in 2- and 1-butanol dehydration, *sec*-butyl-methyl ether cleavage, and 1-butene double-bond isomerization reactions suggest a common *sec*-butoxide intermediate, and, with regard to the alkanol dehydration and ether cleavage reactions, that C−O and C−H bond breakings occur in two subsequent steps. The low kinetic isotope effect of 1.4 measured for 2-propanol-d_8 suggests that none of the X−H bonds are strongly perturbed in the elimination transition state and thus, that the elimination transition states do not involve proton transfer.

n-Donor reactants in alkanol dehydration or ether-decomposition and H_2O products led to reactant and product inhibition effects consistent with the formation of stable and unreactive protonated dimers. The dimer stability is strongly affected by steric repulsion terms.

The effects of DPE of $H_{8-n}X^{n+}W_{12}$ POM clusters on alkanol dehydration rates and elimination barriers are partially masked by the more effective stabilization of the cationic activated complex (carbenium ion) by the deprotonated anionic conjugate base in the case of weaker acids. The differences in ion-pair stabilization point toward differences in the charge density distribution, which are induced mainly by varying numbers of charge balancing protons. Subtle differences in the stabilization of cationic activated complexes or intermediates by the conjugate POM base, which depend on the identity of the acid and specifically on the charge density and distribution in the conjugate base, determine the selectivities in acid-catalyzed reaction networks and the kinetic tolerance to the presence of water and other *n*-donors as reactants, products, or solvents. The energies of cationic transition states and intermediates in Brønsted acid catalyzed reactions reflect DPE values for the acid, protonation enthalpies for reactants or products, and their ion-pair stabilization energies. Both, DPE values and the stabilization energies depend on the identity of the acid and affect transition state energies.

Acknowledgment. Support by the Chemical Sciences, Geo Sciences, Bio Sciences Division, Office of Basic Energy Sciences, Office of Science U.S. Department of Energy under Grant DE-FG02-03ER15479 is gratefully acknowledged. We also thank Dr. Cindy Yin (UC-Berkeley) and Dr. Stuart L. Soled (ExxonMobil) for help with the synthesis of bulk H_5AlW and H_6CoW samples. We acknowledge the use of the computational facilities at the Environmental Molecular Science Laboratory at Pacific Northwest Laboratories (Project 3568).

Supporting Information Available: Complete ref 9; ^{31}P NMR spectra of the H_3PW catalysts, the derivation of the rate equation (eq 2), discussion of the 2-butene selectivity ratios in terms of the energies and partition functions of the intermediates and transition states of the C−H bond breaking step, a figure showing E_a as a function of ΔH^0_{prot} and ΔH^0_{dehy}, two tables with the kinetic parameters for $0.04H_{8-n}X^{n+}W/SiO_2$ (where X = P, Si, Al) and the DFT calculated Mulliken atomic charges for $H_{7-n}X^n{+}O_4^-$, DPEs of $H_{8-n}X^{n+}O_4$, and the interaction energies $E_{int,Na+}$ of $H_{7-n}X^{n+}O_4^-$ and Na^+, respectively. This material is available free of charge via the Internet at http://pubs.acs.org.

JA803114R